

# Boundary element method for nonadhesive and adhesive contacts of a coated elastic half-space

Qiang Li<sup>1</sup> , Roman Pohrt<sup>1</sup>, Iakov A Lyashenko<sup>1,2</sup> and Valentin L Popov<sup>1,3,4</sup>

Proc IMechE Part J:  
J Engineering Tribology  
0(0) 1–11  
© IMechE 2019  
Article reuse guidelines:  
sagepub.com/journals-permissions  
DOI: 10.1177/1350650119854250  
journals.sagepub.com/home/pij



## Abstract

We present a new formulation of the boundary element method for simulating the nonadhesive and adhesive contact between an indenter of arbitrary shape and an elastic half-space coated with an elastic layer of different material. We use the Fast Fourier Transform-based formulation of boundary element method, while the fundamental solution is determined directly in the Fourier space. Numerical tests are validated by comparison with available asymptotic analytical solutions for axisymmetric flat and spherical indenter shapes.

## Keywords

Boundary element method, coated elastic body, adhesive contact, contact mechanics, coatings

Date received: 30 July 2018; accepted: 10 May 2019

## Introduction

Layered systems of materials having different mechanical properties have attracted a lot of scientific interest over the last decades.<sup>1,2</sup> A well-chosen coating can improve the structural, mechanical, optical, or thermal properties at the surface of a bulk material. Layered structure can be created by ion implantation, vacuum deposition, nanostructure burnishing, laser implantation, and other manufacturing technologies. Coatings are widely used e.g. for reducing wear, increasing corrosion resistance, controlling friction, influencing adhesion properties, or manipulating thermal. Due to the significant influence surface layers have on mechanical properties, a multitude of experimental techniques has been developed for the characterization of coatings, in particular measuring their elastic properties.<sup>3</sup>

For the case of nonadhesive elastic contact with coated systems, theoretical solutions of various indenters have been obtained. These solutions range from the early asymptotic solution for line and circular contacts on a single layer coating on an otherwise rigid foundation,<sup>4,5</sup> to the semi-analytical solution for axisymmetric contacts on a general multilayer substrate.<sup>6</sup> Usually the integral transform method or images method are used for achieving an analytical solution.<sup>7,8</sup> The adhesive contact between a rigid sphere and an elastic multilayer coated half-space was investigated by use of an integral transform formulation

and Maugis-type adhesion model.<sup>9</sup> Solutions for axisymmetric contacts on a single layer were found using a JKR-type (Johnson–Kendall–Roberts) adhesion model.<sup>10</sup> For a randomly rough surface in contact with a coated half-space only approximate analytical theory is available.<sup>11</sup>

Numerical methods have also been intensively developed to study the contact and tribological behavior of layered materials. The finite element method (FEM) is most commonly used. It is very versatile and can be applied for various structures without the restriction of linear material behavior. In contrast to FEM, the Fast Fourier Transforms (FFT)-based boundary element method (BEM) is suitable for all problems where the elastic and geometrical behavior is linear. In part because of its much higher numerical efficiency for contact problems, the BEM evolved to be the standard method in research and development. The boundary element formulation was presented for a contact of an arbitrary shaped indenter with a homogeneous half-space.<sup>12</sup> Later,

<sup>1</sup>Berlin University of Technology, Berlin, Germany

<sup>2</sup>Sumy State University, Sumy, Ukraine

<sup>3</sup>National Research Tomsk State University, Tomsk, Russia

<sup>4</sup>National Research Tomsk Polytechnic University, Tomsk, Russia

## Corresponding author:

Valentin L Popov, Technische Universität Berlin, Str. des 17. Juni, Berlin 10623, Germany.

Email: v.popov@tu-berlin.de

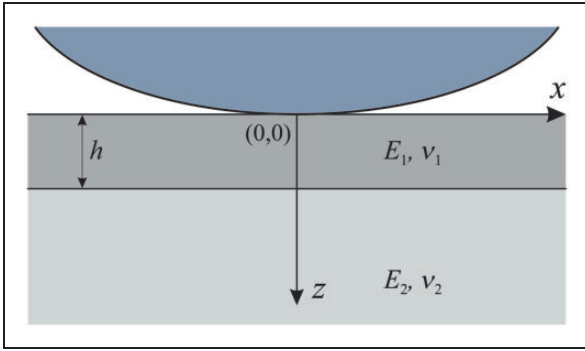


**Figure 1.** Scheme of the system under consideration. An elastic layer with thickness  $h$ , elastic modulus  $E_1$ , and Poisson ratio  $\nu_1$  is located on top of an elastic half-space with elastic parameters  $E_2$  and  $\nu_2$ .

it was extended to include JKR-type adhesion.<sup>13</sup> The method was validated by available analytical solutions including parabolic contacts (classical JKR solution), toroidal indenters,<sup>14</sup> and flat elliptical indenters.<sup>15</sup> Recently, it was also applied to contacts between flat-ended indenters of complicated shape and a flat soft body.<sup>16</sup> The BEM was extended also to include contacts with power-law graded materials.<sup>17</sup>

In the present paper, we propose a further generalization of BEM for the case of a coated half-space. Several numerical tests will be carried out and the results will be compared with the known analytical solutions.

### FFT-based BEM for layered half-space

We consider a half-space with a single elastic coating of thickness  $h$ , elastic modulus  $E_1$  and Poisson ratio  $\nu_1$ . The corresponding elastic constants of the half-space are  $E_2$  and  $\nu_2$  (Figure 1). The origin of coordinates is placed at the surface of the layer so that the interface between two media is located at  $z = h$ .

In previous versions of the BEM for contact of homogeneous and power-law graded materials,<sup>12,17</sup> we proceeded from the fundamental solution in coordinate space and the corresponding integral formulation of the stress–displacement relation. This integral relation has the form of a convolution of the surface pressure distribution with the fundamental solution  $\mathbf{U}_0$ . This fundamental solution represents the deformation resulting from a single localized normal force. For the numerical solution of the contact problem, we consider a square region on the surface of the body with the size  $L \times L$ , discretized with  $N$  cells in each direction. The size of each of the  $N^2$  square cells is  $\Delta x = \Delta y = \Delta$ . Pressure is assumed to be uniform in each cell (see Figure 2).

In the discretized form, the pressure–displacement relation can be written as

$$\mathbf{u} = \mathbf{K}\mathbf{p} \quad (1)$$

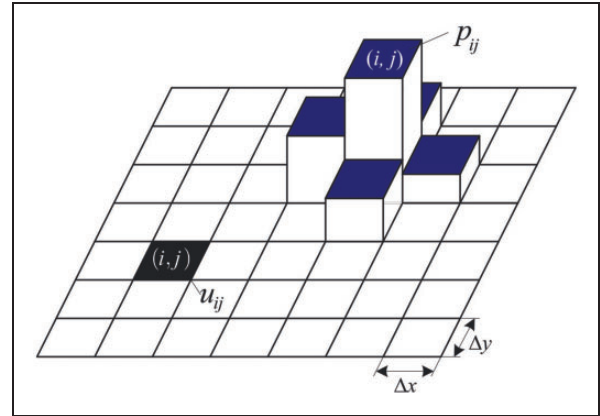


**Figure 2.** Discretization of the simulation area.

where  $\mathbf{p}$  is stress distribution acting on the surface (vector of the length  $N^2$  with values of pressure in the corresponding discrete cells),  $\mathbf{u}$  is the normal displacement of surface elements due to applied pressure, and  $\mathbf{K}$  is the compliance matrix having the size  $N^4$ . The contact problem is solved in BEM iteratively. In each step, the displacements for a given (assumed) pressure distribution are determined by evaluation of equation (1). Because of the convolution-type integral equation and the resulting structure of matrix  $\mathbf{K}$ , the operation is performed using direct and inverse FFT

$$\mathbf{u} = \text{IFFT}[\text{FFT}(\mathbf{U}_0) \cdot \text{FFT}(\mathbf{p})] \quad (2)$$

The number of operation for performing this operation is on the order of  $O(N^2 \log N)$  (as compared with  $O(N^4)$  for direct evaluation of equation (1)).

The compliance matrix  $\mathbf{K}$  is basically a long version of the discretized fundamental solution of the problem. To be used in equation (2), a known fundamental solution  $\mathbf{U}_0$  must first be Fourier-transformed. However, if the fundamental solution can be found directly in the Fourier space, this step could be omitted. In the present paper, we determine the fundamental solution for a layered system directly in the Fourier space in analytic form thus saving both one Fourier transform and memory space.

For the derivation of the fundamental solution in Fourier space, we consider a pressure distribution acting on the surface of the layer in the form of a plane wave with wave vector  $\mathbf{k}$  and amplitude  $p_0$

$$p = p_0 e^{i\mathbf{k}\mathbf{r}} \quad (3)$$

Here  $\mathbf{r}$  is the (two-dimensional) radius vector in the contact plane. Here and further in the text non-bold symbol,  $k$  denotes the absolute values of vector,  $k = |\mathbf{k}|$ . For simplicity, without loss of generality, let us use the direction of wave vector  $\mathbf{k}$  as the  $x$ -axis, thus  $e^{i\mathbf{k}\mathbf{r}} = e^{ikx}$  and equation (3) can be simplified as  $p = p_0 e^{i\mathbf{k}\mathbf{r}} = p_0 e^{ikx}$ .

In the homogeneous case, with  $E_1 = E_2 = E$  and  $\nu_1 = \nu_2 = \nu$ , the vertical displacement of the surface ( $z = 0$ ) is given by<sup>18</sup>

$$u_z(x, y) = u_z(k)e^{ikx} \quad \text{with} \quad u_z(k) = \frac{2p_0}{E^*k} \quad (4)$$

where  $E^*$  is the reduced elastic modulus  $E^* = E/(1-\nu^2)$ . In the following, we provide the corresponding solution for a layered system.

The equilibrium equation of an elastic isotropic medium reads<sup>19</sup>

$$\text{grad div } \mathbf{u} + (1 - 2\nu_{1,2})\nabla^2 \mathbf{u} = 0 \quad (5)$$

where  $\nu_1$  is the Poisson number of the layer and  $\nu_2$  that of the half-space. The displacement vector  $\mathbf{u}$  will also have the form of a plane wave

$$\mathbf{u} = u_x \mathbf{e}_x + u_y \mathbf{e}_y + u_z \mathbf{e}_z = u_x^0(z)e^{ikx} \mathbf{e}_x + u_z^0(z)e^{ikx} \mathbf{e}_z \quad (6)$$

Here  $\mathbf{e}_x$  and  $\mathbf{e}_z$  are unit vectors in directions of the wave vector and perpendicular to the contact plane correspondingly. Symbols  $u_x$ ,  $u_y$  and  $u_z$  denote projections of the displacement vector on the corresponding directions. The projection in  $y$  direction is zero,  $u_y = 0$ . The amplitudes  $u_x^0$  and  $u_z^0$  are only functions of the vertical coordinate  $z$ .

Operators appearing in equation (5) read

$$\begin{aligned} \text{div } \mathbf{u} &= \frac{\partial}{\partial x} [u_x^0(z)e^{ikx}] + \frac{\partial}{\partial z} [u_z^0(z)e^{ikx}] \\ &= ik u_x^0(z)e^{ikx} + \frac{\partial u_z^0(z)}{\partial z} e^{ikx} \end{aligned} \quad (7)$$

$$\begin{aligned} \text{grad div } \mathbf{u} &= \left[ -k^2 u_x^0(z)e^{ikx} + ik \frac{\partial u_z^0(z)}{\partial z} e^{ikx} \right] \mathbf{e}_x \\ &\quad + \left[ ik \frac{\partial u_x^0(z)}{\partial z} e^{ikx} + \frac{\partial^2 u_z^0(z)}{\partial z^2} e^{ikx} \right] \mathbf{e}_z \end{aligned} \quad (8)$$

$$\begin{aligned} \nabla^2 \mathbf{u} &= \left( \frac{\partial^2}{\partial x^2} + \frac{\partial^2}{\partial z^2} \right) [u_x^0(z)e^{ikx}] \mathbf{e}_x \\ &\quad + \left( \frac{\partial^2}{\partial x^2} + \frac{\partial^2}{\partial z^2} \right) [u_z^0(z)e^{ikx}] \mathbf{e}_z \\ &= \left[ -k^2 u_x^0(z)e^{ikx} + \frac{\partial^2 u_x^0(z)}{\partial z^2} e^{ikx} \right] \mathbf{e}_x \\ &\quad + \left[ \frac{\partial^2 u_z^0(z)}{\partial z^2} e^{ikx} - k^2 u_z^0(z)e^{ikx} \right] \mathbf{e}_z \end{aligned} \quad (9)$$

After substitution of these expressions into equation (5), we have the following relations

$$\frac{\partial^2 u_x^0(z)}{\partial z^2} + \frac{ik}{1-2\nu_{1,2}} \frac{\partial u_z^0(z)}{\partial z} - \frac{2(1-\nu_{1,2})k^2}{1-2\nu_{1,2}} u_x^0(z) = 0 \quad (10)$$

$$\frac{\partial^2 u_z^0(z)}{\partial z^2} - \frac{ik}{2(\nu_{1,2}-1)} \frac{\partial u_x^0(z)}{\partial z} + \frac{(1-2\nu_{1,2})k^2}{2(\nu_{1,2}-1)} u_z^0(z) = 0 \quad (11)$$

We search solution of this system in the form

$$u_x^0(z) = Ae^{\lambda z}; \quad u_z^0(z) = Be^{\lambda z} \quad (12)$$

Substitution of equation (12) into equations (10) and (11) gives

$$A\lambda^2 + B \frac{ik}{1-2\nu_{1,2}} \lambda - \frac{2(1-\nu_{1,2})k^2}{1-2\nu_{1,2}} A = 0 \quad (13)$$

$$B\lambda^2 - \frac{ik}{2(\nu_{1,2}-1)} A\lambda + \frac{(1-2\nu_{1,2})k^2}{2(\nu_{1,2}-1)} B = 0 \quad (14)$$

The systems (13) and (14) have only trivial solution if its determinant vanishes

$$\begin{vmatrix} \lambda^2 - \frac{2(1-\nu_{1,2})k^2}{1-2\nu_{1,2}} & \frac{ik}{1-2\nu_{1,2}} \lambda \\ -\frac{ik}{2(\nu_{1,2}-1)} \lambda & \lambda^2 + \frac{(1-2\nu_{1,2})k^2}{2(\nu_{1,2}-1)} \end{vmatrix} = 0 \quad (15)$$

This characteristic equation has four roots  $\lambda_{1,2,3,4} = k, -k, k, -k$ . Thus the general solution has the form

$$\begin{aligned} u_z^{(1)}(x, z) &= u_z^0(z)e^{ikx} \\ &= (A_1 e^{kz} + A_2 e^{-kz} + A_3 z e^{kz} + A_4 z e^{-kz}) e^{ikx} \end{aligned} \quad (16)$$

$$\begin{aligned} u_x^{(1)}(x, z) &= u_x^0(z)e^{ikx} \\ &= (B_1 e^{kz} + B_2 e^{-kz} + B_3 z e^{kz} + B_4 z e^{-kz}) e^{ikx} \end{aligned} \quad (17)$$

inside the coating ( $0 \leq z \leq h$ ) and the same general form with another set of coefficients inside the half-space ( $z > h$ )

$$\begin{aligned} u_z^{(2)}(x, z) &= u_z^0(z)e^{ikx} \\ &= (A_5 e^{kz} + A_6 e^{-kz} + A_7 z e^{kz} + A_8 z e^{-kz}) e^{ikx} \end{aligned} \quad (18)$$

$$\begin{aligned} u_x^{(2)}(x, z) &= u_x^0(z)e^{ikx} \\ &= (B_5 e^{kz} + B_6 e^{-kz} + B_7 z e^{kz} + B_8 z e^{-kz}) e^{ikx} \end{aligned} \quad (19)$$

The superscripts (1) and (2) indicate the coating and half-space respectively. There are 16 coefficients to be determined. Substitution of  $u_z^0(z)$  and  $u_x^0(z)$  in equations (16)–(19) into the differential equations (10) and (11) generates

$$\begin{aligned} B_1 &= i \left( A_1 + \frac{A_3(3-4\nu_1)}{k} \right), \\ B_2 &= -i \left( A_2 - \frac{A_4(3-4\nu_1)}{k} \right), \quad B_3 = iA_3, \quad B_4 = -iA_4 \end{aligned} \quad (20)$$

$$\begin{aligned}
B_5 &= i \left( A_5 + \frac{A_7(3-4v_2)}{k} \right), \\
B_6 &= -i \left( A_6 - \frac{A_8(3-4v_2)}{k} \right), \quad B_7 = iA_7, \quad B_8 = -iA_8
\end{aligned} \quad (21)$$

We use the following boundary conditions:

- Displacements of half-space at infinite depth are zero:  $u_x^{(2)}(x, z \rightarrow \infty) = 0$  and  $u_z^{(2)}(x, z \rightarrow \infty) = 0$ ;
- Continuity of displacements at the interface between the half-space and coating:  $u_z^{(1)}(x, h) = u_z^{(2)}(x, h)$ ,  $u_x^{(1)}(x, h) = u_x^{(2)}(x, h)$ ;
- Vanishing of tangential stresses at the contact plane (frictionless problem):  $\tau_{zx}^{(1)}(x, 0) = 0$ ;
- Given normal stress distribution at the surface, equation (3):  $\sigma_{zz}^{(1)}(x, z = 0) = -p_0 e^{ikx}$ ;
- Continuity of stresses and strains at the interface between the half-space and coating:  $\sigma_{zz}^{(1)}(x, h) = \sigma_{zz}^{(2)}(x, h)$ ,  $\tau_{zx}^{(1)}(x, h) = \tau_{zx}^{(2)}(x, h)$ .

The first boundary condition (a) leads to

$$A_5 = 0, \quad A_7 = 0, \quad B_5 = 0, \quad B_7 = 0 \quad (22)$$

and the others lead to the system of linear algebraic equations

$$\frac{\left\{ \begin{aligned} &E_1[A_1k(1-2v_1) + A_2k(-1+2v_1)] \\ &+ A_3(1-4v_1+4v_1^2) + A_4(1-4v_1+4v_1^2) \end{aligned} \right\}}{(1+v_1)(1-2v_1)} = -p_0 \quad (23)$$

$$A_1 e^{2kh} + A_2 + A_3 h e^{2kh} + A_4 h - A_6 - A_8 h = 0 \quad (24)$$

$$\begin{aligned}
&[kA_1 + A_3(3-4v_1+kh)]e^{2kh} - kA_2 \\
&+ A_4(3-4v_1-kh) + kA_6 - A_8(3-4v_2-kh) = 0
\end{aligned} \quad (25)$$

$$\begin{aligned}
&\frac{E_1}{(1+v_1)(1-2v_1)} \left[ e^{2kh}(A_1k(1-2v_1) \right. \\
&+ A_3(1+kh-4v_1-2v_1kh+4v_1^2)) \\
&+ A_2k(-1+2v_1) \\
&+ A_4(1-kh-4v_1+2v_1kh+4v_1^2) \\
&- \frac{E_2}{(1+v_2)(1-2v_2)} [A_6k(-1+2v_2) \\
&+ A_8(1-kh-4v_2+2v_2kh+4v_2^2)] = 0
\end{aligned} \quad (26)$$

$$\begin{aligned}
&\frac{E_1}{(1+v_1)} [(A_1k + A_3(2-2v_1+kh))e^{2kh} \\
&+ A_2k + A_4(-2+2v_1+kh)] \\
&- \frac{E_2}{(1+v_2)} [A_6k + A_8(-2+2v_2+kh)] = 0
\end{aligned} \quad (27)$$

$$A_1k + A_2k + 2A_3(1-v_1) + 2A_4(-1+v_1) = 0 \quad (28)$$

For the plain normal contact problem, we only need normal displacements at the contact surface. The solution of the systems (23)–(28) can be substituted into equation (16) and we obtain

$$\begin{aligned}
&u_z(x, z = 0) \\
&= \frac{2p_0(1-v_1^2)(Ae^{-4kh} + Bkhe^{-2kh} + D)}{kE_1(-Ae^{-4kh} - Bk^2h^2e^{-2kh} + 2Ce^{-2kh} + D)} e^{ikx}
\end{aligned} \quad (29)$$

where the constants  $A$ ,  $B$ ,  $C$ ,  $D$  are given by the following expressions

$$\begin{aligned}
A &= [E_2(3-4v_1)(1+v_1) - E_1(3-4v_2)(1+v_2)] \\
&\cdot [E_1(1+v_2) - E_2(1+v_1)] \\
B &= 4[E_2(1+v_1) + E_1(3-4v_2)(1+v_2)] \\
&\cdot [E_1(1+v_2) - E_2(1+v_1)] \\
C &= E_1^2(4v_2-3)(1+v_2)^2 \\
&- 2E_1E_2(v_1+1)(2v_1-1)(v_2+1)(2v_2-1) \\
&+ E_2^2(8v_1^2-12v_1+5)(1+v_1)^2 \\
D &= [E_2(1+v_1) + E_1(3-4v_2)(1+v_2)] \\
&\cdot [E_2(3-4v_1)(1+v_1) + E_1(1+v_2)]
\end{aligned} \quad (30)$$

For any given pressure distribution  $\mathbf{p}$ , the vertical displacement of the surface at  $z = 0$  can now be calculated explicitly using equation (29)

$$\mathbf{u} = \mathbf{IFFT} \left[ \frac{2(1-v_1^2)}{E_1} \frac{Ae^{-4kh} + Bkhe^{-2kh} + D}{\left\{ \begin{aligned} &k(-Ae^{-4kh} - Bk^2h^2e^{-2kh}) \\ &+ 2Ce^{-2kh} + D \end{aligned} \right\}} \cdot \mathbf{FFT}(\mathbf{p}) \right] \quad (31)$$

Note that the middle item in the square bracket is the function of  $k$ . For some certain  $k$ , it is constant and one can consider it as the coefficient of the term  $\mathbf{FFT}(\mathbf{p})$  for the corresponding value of  $k$ . Numerically both terms are 2D matrices and the operation  $\langle \cdot \rangle$  will then be element-wise multiplication. Similar to equation (4), this procedure only gives results for  $k \neq 0$ , in other words, the pressure distribution must have no DC component. The usual BEM procedure reduces to performing the FFT of pressure distribution, multiplying the result with the analytical fundamental solution (equation (29)) and performing inverse FFT to find the displacement field. The inverse problem of finding pressure for producing given deformations can be solved by the conjugate graded method.<sup>12</sup> Conjugate graded method is a widely used numerical algorithm for solution of systems of linear equations, and it has been used in contact problems

frequently. A detailed discussion of this method and its extension in contact mechanics can be found in the paper.<sup>20</sup> Proper preconditioning<sup>20</sup> allows keeping the number of iteration steps of the procedure bounded by approximately 10 independently of the complexity of contact configuration and mesh size. These two steps complete the formulation of BEM for nonadhesive contacts with layered systems. For adhesive contacts, an additional detachment criterion is needed which is discussed in the remainder of this section.

In each step of an adhesive BEM simulation, the pressure distribution is calculated in all discretized grid cells and it has to be decided whether each point remains in contact or detaches. In Pohrt and Popov<sup>13</sup> and Popov et al.,<sup>16</sup> it was suggested to make the decision based on the energy balance criterion of Griffith.<sup>21</sup> For a nonperiodic system of a homogenous elastic half-space and a rigid indenter, this leads to a local mesh-dependent detachment criterion: A surface element at the boundary of the contact loses its contact as soon as tensile stress in this element exceeds the critical value given by

$$\sigma_c = \sqrt{\frac{E_1^* \Delta \gamma}{0.473201 \cdot \Delta}} \quad (32)$$

Here  $\Delta \gamma$  is the specific work of adhesion between the indenter and substrate, and  $E_1^* = E_1 / (1 - \nu_1^2)$ . Note that this criterion contains only elastic properties of the coating. This criterion applies also to layered systems, as long as the size  $\Delta$  of the discrete cell is much smaller than the thickness of the layer. Under this assumption, the elastic energy released due to the detachment of an element is completely ‘‘confined’’ in the coating, thus the detachment criterion has the same form as in the case of the homogeneous material<sup>9,12</sup> with elastic properties of the coating.

The calculation procedure for numerical simulation of an adhesive contact is basically the same as for nonadhesive contacts. The main difference is in the condition for the loss of contact. Instead of requiring all normal stresses to satisfy  $p > 0$ , the condition  $p > -\sigma_c$  is imposed. Because the adhesive solution is potentially not unique, we can only approach it from the state of full contact.

If the entire detachment process is considered, then starting from full contact, the indenter is moved upwards by a distance  $\Delta d$  (displacement-controlled pull off) in each step. First it is assumed that the contact area does not change, so that all displacements of contact points are augmented by  $\Delta d$ . In the second stage, the new stress distribution  $p'$  is calculated, which satisfies the new displacement field (inverse problem). In the third stage, stresses are checked in all elements at the boundary of the contact area. If the tensile stress in an element is larger than the critical value (32), this element detaches (the stress is set zero), and a reduced contact area  $A'$  is obtained. The stress distribution is calculated again with the new contact

area and the contact criterion is checked again. This iteration procedure is continued until the tensile stress in each element is smaller than  $\sigma_c$  in (32) which means that the correct contact zone and stresses have been found. Then the simulation continues with the next pull-off step.

## Numerical results and comparison with analytic solutions

In recent studies,<sup>10,22,23</sup> it was shown that the solution for axis-symmetric adhesive contact problems can be deduced from the solution of the nonadhesive contact problem: The critical separation distance  $d_c$  in adhesive contact is determined by the equation

$$\frac{dk_s(a) d_c^2}{da} = 2\pi a \Delta \gamma \quad (33)$$

where  $k_s(a)$  is the dependency of the incremental stiffness on the contact radius  $a$  for the *nonadhesive* contact problem. Let us apply this relation to the limiting case of an elastic layer bonded to a rigid substrate. The asymptotically exact result in this case with the additional condition  $a \gg h$  is given by<sup>24</sup>

$$k_s = \frac{\pi a^2}{h} \tilde{E}_1 \quad (34)$$

$$\tilde{E}_1 = E_1 \frac{1 - \nu_1}{(1 + \nu_1)(1 - 2\nu_1)} \quad (35)$$

Substitution into equation (33) provides the following critical values for the indentation depth and the pull-off force.

$$d_c = -\sqrt{\frac{2\Delta\gamma h}{\tilde{E}_1}}, \quad F_c = k_s d_c = -\pi a^2 \sqrt{\frac{2\tilde{E}_1 \Delta \gamma}{h}} \quad (36)$$

In the frame of the proposed BEM formulation, we can simulate this limiting case by assuming a very large ratio of  $E_2/E_1$ . Simulation results of the pull off of a flat cylindrical indenter are shown in Figure 3 for two ratios  $E_2/E_1 = 10^5$  and  $E_2/E_1 = 10^2$  with  $E_1 = 2 \cdot 10^9$  Pa,  $\nu_1 = \nu_2 = 0.3$  and  $a = 50h$ . The displacement and the force are normalized to the critical values (36):  $\tilde{F} = F/|F_c|$  vs  $\tilde{d} = d/|d_c|$ . As expected, the force-displacement relation is linear up to the moment of sudden complete detachment. In the case of  $E_2/E_1 = 10^2$ , this instability point does not match the critical values (36)  $\tilde{F} = -1$  and  $\tilde{d} = -1$ . This is due to the fact that the two ratios  $E_2/E_1$  and  $a/h$  are of the same order of magnitude. Therefore, the asymptotic solution is not suitable for predicting the detachment. For  $E_2/E_1 = 10^5$ , the condition for the asymptotical solution is satisfied, thus it can be used to validate the correctness of our numerical criterion. Indeed, at the point of sudden detachment, the normalized numerical values approach  $(-1, -1)$  very closely.

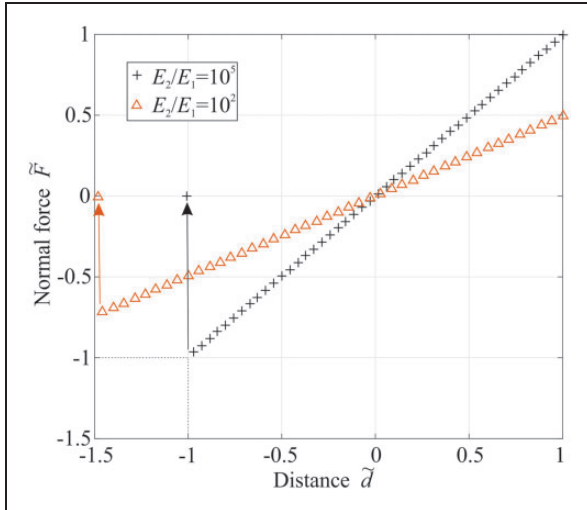


**Figure 3.** Dependencies of the dimensionless elastic force vs. dimensionless distance for the adhesive contact of a cylindrical indenter on an elastic layer.

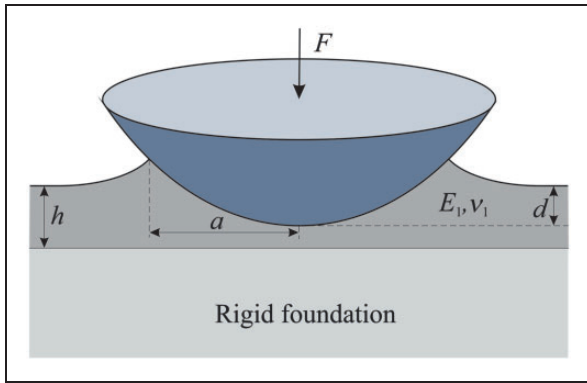


**Figure 4.** Adhesive contact between a rigid indenter and an elastic layer bound to a rigid foundation.

### Indentation of a parabolic indenter

For a thin elastic layer, an asymptotically exact analytic solution exists for arbitrary indenter shapes provided the condition  $a \gg h$  is satisfied. In the limiting case,  $E_2 \rightarrow \infty$ , displayed in Figure 4, the solution for a parabolic indenter reads<sup>10,25</sup>

$$F = \frac{\pi \tilde{E}_1 a^2}{h} \left( \frac{a^2}{4R} - \sqrt{\frac{2\Delta\gamma h}{\tilde{E}_1}} \right) \quad (37)$$

$$d = \frac{a^2}{2R} - \sqrt{\frac{2\Delta\gamma h}{\tilde{E}_1}} \quad (38)$$

The critical values of force, separation, and contact radius are given by

$$d_{crit} = -\sqrt{\frac{2\Delta\gamma h}{\tilde{E}_1}}, \quad a_{crit} = \left( \frac{8R^2 h \Delta\gamma}{\tilde{E}_1} \right)^{1/4}, \quad F_{crit} = -2\pi R \Delta\gamma \quad (39)$$

With dimensionless variables,  $\tilde{a} = \frac{a}{a_{crit}}$ ,  $\tilde{d} = \frac{d}{|d_{crit}|}$ ,  $\tilde{F} = \frac{F}{|F_{crit}|}$ , the dependencies of the normal force on indentation depth and contact radius (37) and (38) can be written in the form

$$\tilde{F} = \tilde{a}^4 - 2\tilde{a}^2 \quad (40)$$

$$\tilde{d} = \tilde{a}^2 - 1 \quad (41)$$

These relations are plotted with a black dashed line in Figure 5(a) and (b). The corresponding numerical results are shown by the curve with “plus” symbols for the case of  $\alpha = 15$ , which we will define later in equation (47), now indicating the case of  $a \gg h$ . The other parameters can be found in the following discussion. Numerical and asymptotical solutions are a very close match. The small discrepancy may again be due to finite values of  $E_2/E_1$  and  $a/h$  used in the numerical simulation.

In the opposite limiting case of the contact radius being small compared to the thickness of the layer, analytical solutions exist in form of asymptotic series<sup>26</sup> in dimensionless parameter  $\varepsilon = a/h \ll 1$

$$F = \frac{4E_1^* a^3}{3R} \left( 1 - \varepsilon^3 \frac{8a_1}{3\pi} \right) \left( 1 - \frac{3R\sqrt{2\pi E_1^* a \Delta\gamma}}{2E_1^* a^2} \right) \quad (42)$$

$$d = \frac{a^2}{R} \left[ 1 - \varepsilon \frac{4a_0}{3\pi} - \varepsilon^3 \frac{16a_1}{5\pi} + \varepsilon^4 \frac{32a_0 a_1}{9\pi^2} - \frac{R\sqrt{2\pi E_1^* a \Delta\gamma}}{E_1^* a^2} \left( 1 - \varepsilon \frac{2a_0}{\pi} - \varepsilon^3 \frac{16a_1}{3\pi} + \varepsilon^4 \frac{16a_0 a_1}{3\pi^2} \right) \right] \quad (43)$$

The coefficients in equations (42) and (43) are given by

$$a_m = \frac{(-1)^m}{2^{2m} (m!)^2} \int_0^\infty \Lambda(u) u^{2m} du \quad (44)$$

$$\Lambda(u) = \frac{2KLe^{-4u} - (L + K + 4uK + 4u^2K)e^{-2u}}{1 - (L + K + 4u^2K)e^{-2u} + KLe^{-4u}} \quad (45)$$

with coefficients

$$K = \frac{1-n}{1+n(3-4\nu_1)}, \quad L = \frac{(3-4\nu_2) - n(3-4\nu_1)}{(3-4\nu_2) + n}, \quad n = \frac{E_2(1+\nu_1)}{E_1(1+\nu_2)} \quad (46)$$

The dependencies (42) and (43) for  $F$  and  $d$  depend on the following adhesion parameter<sup>24,26</sup>

$$\alpha = \sqrt{\frac{2\Delta\gamma R^2}{E_1^* h^3}} \quad (47)$$

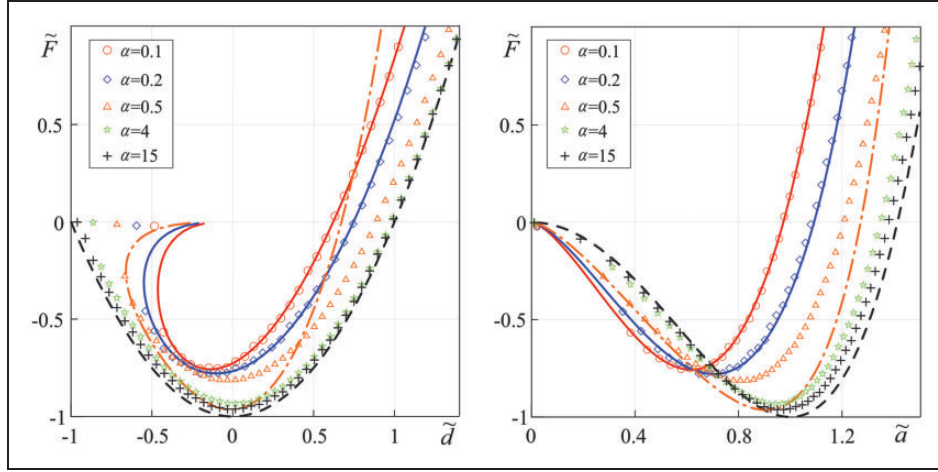


**Figure 5.** Dependencies of dimensionless contact force on dimensionless indentation depth and contact radius, for the adhesive indentation of a spherical indenter into a layered counter body. Curves for different values of adhesion parameter  $\alpha$  are shown. Dashed lines depict the dependencies (40) and (41) for the case of  $a \gg h$ . Dash-dot and solid lines are given by expressions (42) and (43) for the case of  $a \ll h$ . Symbols are numerical results obtained by the BEM presented in this paper.

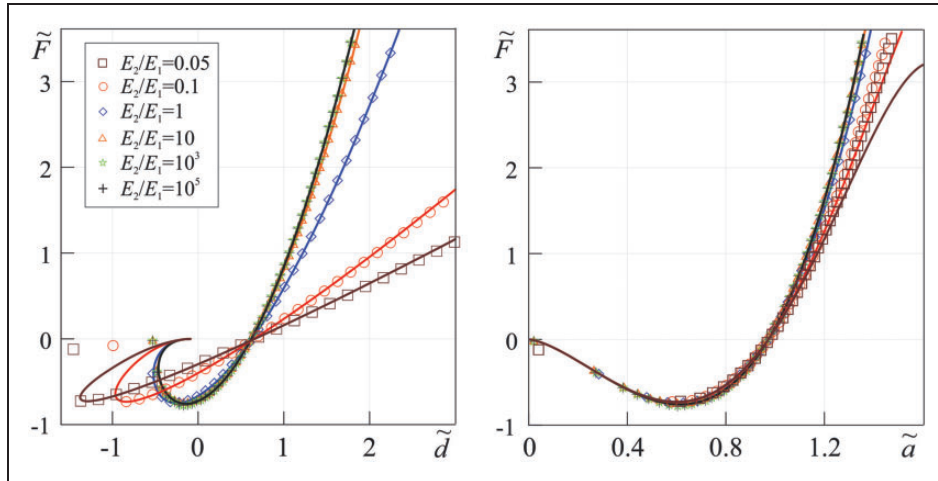


**Figure 6.** (a) Force–displacement and (b) force–contact radius relation for different ratios of  $E_2/E_1$ .

Numerically we carried out the pull-off simulation with five different adhesion parameters  $\alpha$  ranging from 0.1 to 15, where the constant parameters are set as  $E_1 = 10^9$  Pa,  $E_2 = e^{100}$  Pa (which means  $\infty$ , corresponding to the limiting case of rigid foundation),  $\nu_1 = 0.3$ ,  $h = 2$  mm,  $\Delta\gamma = 100$  J/m<sup>2</sup> and  $\alpha$  is varied by changing the radius of curvature  $R$  of the indenter. The results are shown in Figure 5 in the same dimensionless coordinates as given by equations (40) and (41). The curves for  $\alpha = 0.1$  and 0.2 corresponding to small contact radii are compared with the asymptotic relations (42) and (43) while that of large parameter  $\alpha$  are compared with the asymptotic relations (40) and (41). In both limiting cases, we see very good agreement between numerical and analytical results. For intermediate values of  $\alpha$  an interesting behavior can be observed. For example in the case of  $\alpha = 0.5$ , for the small indentation depth when the contact

radius is much smaller than the layer thickness  $a \ll h$ , a good coincidence can be observed between numerical (triangles) and analytical results (dash-dot line). With an increasing indentation depth, the analytical solution is not valid any more. At large indentation depths, the numerical results approach the dashed line (the other limiting case  $a \gg h$ ) due to a large contact radius. We thus conclude that numerical results coincide with all available analytical results in region of their validity.

Instead of varying the adhesive parameter, let us now look at the influence of the elastic parameters of the foundation on the detachment process. The approximate equations (42) and (43) provide results with a high accuracy (see Figure 5) for low values of  $\alpha$ . We choose fixed values  $\alpha = 0.1$  and  $R \approx 21$  mm with the other parameters identical as in the above case but at varying values of  $E_2/E_1$ . Results for

$\tilde{F}$  over  $\tilde{d}$  and  $\tilde{a}$  are shown in Figure 6 and coincide with analytical approximation very well for different values of  $E_2/E_1$ .

From Figure 6 it can be seen that with increasing ratio of elastic moduli  $E_2/E_1$  the dependencies become universal, as the limit of a very rigid half-space is approached (see Figure 5). Note that in the case of  $E_2/E_1 = 0.05$ , analytical approximation (solid line) gives wrong result in the range of a large contact radius ( $\tilde{a} > 1.25$ ) due to the limitation  $a \ll h$ , (see upper limit of Figure 6(b)).

### Case studies of flat-ended indenters

Here we present two applications of the above-validated numerical method: The indentation test of a square punch on stiff coatings and the adhesive pull off of a star-shaped indenter. Both are non-axisymmetric contact problems and analytical solutions are not available.

#### Indentation of a square punch on hard coatings

We consider a nonadhesive contact between a square indenter with length  $L_0$  and an elastic half space coated by a stiff layer ( $E_2/E_1 < 1$ ). We put special focus on the contact area  $A$ . For the homogeneous contact, it is known that the contact area is simply the area of the full square,  $A_0$ . However, when we introduce a stiff coating, an interesting behavior can be observed in the indentation test. If the stiff layer is thin and the foundation is relatively soft, then the indentation leads to the loss of contact in the middle of the square (Figure 7(a)). Because of linearity, the contact area is independent of the indentation depth. Figure 7(a) shows the dependency of  $A/A_0$

on the ratio of  $E_2/E_1$  for the case of  $h/L_0 = 0.5$ . It can be seen that the contact area decreases with decreasing ratio  $E_2/E_1$  (stiffer layer) and finally approaches a constant plateau. At the plateau, the contact zone is limited by the edges of the initial square. There is a critical value of  $E_2/E_1$  dividing the cases of partial and full contact, e.g.  $E_2/E_1 \approx 0.15$ , for the case of the layer thickness  $h/L_0 = 0.5$ . Figure 7(b) shows that this critical value is dependent of the relative layer thickness: for a thinner layer, full contact can be achieved with a softer layer material. For a thick layer  $h/L_0 = 0.9$ , the contact is always complete because the deformation occurs mainly in the layer. We also find that in the case of a very thin layer  $h/L_0 = 0.1$  another behavior can be observed: contact exists both in the center and at edges (see inset picture in Figure 7(b)).

The described multiple contact behavior has been observed in the analytical<sup>27,28</sup> and in numerical studies<sup>29</sup> for indentation problem of a layered medium by a rigid one-dimensional (infinite long) flat punch. It was found that the multiple contact appears only in the case of stiff layer and soft half space, and the solutions to the full contact, border contact, and border center contact depends on the material and geometrical properties, not on the indentation depth. For the complicated form of indenters (e.g., the studied case) an analytical solution is not possible, but the BEM shows that behavior is similar to that of simpler geometries.

#### Adhesive contact of a star-shaped indenter

The adhesive detachment of a flat indenter with odd shape from a homogeneous elastic half space has been studied in Popov et al.<sup>16</sup> It was found that flat

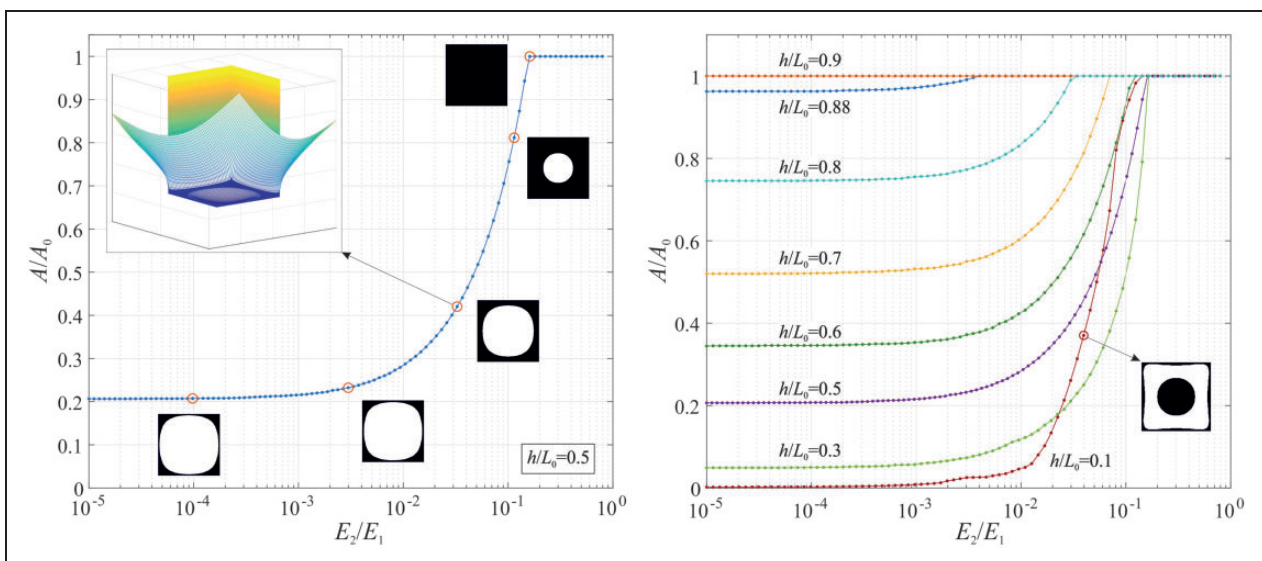


**Figure 7.** (a) Dependency of contact area on the ratio of elastic moduli  $E_2/E_1$ . Inset pictures show the contact areas (black color) at the given ratio. The color picture in the upper left shows a sample contact configuration of the square indenter and the deformed surface of the layer, with a noncontact bump in the center. (b) Same as (a) but for different values of the relative layer thickness  $h$ .

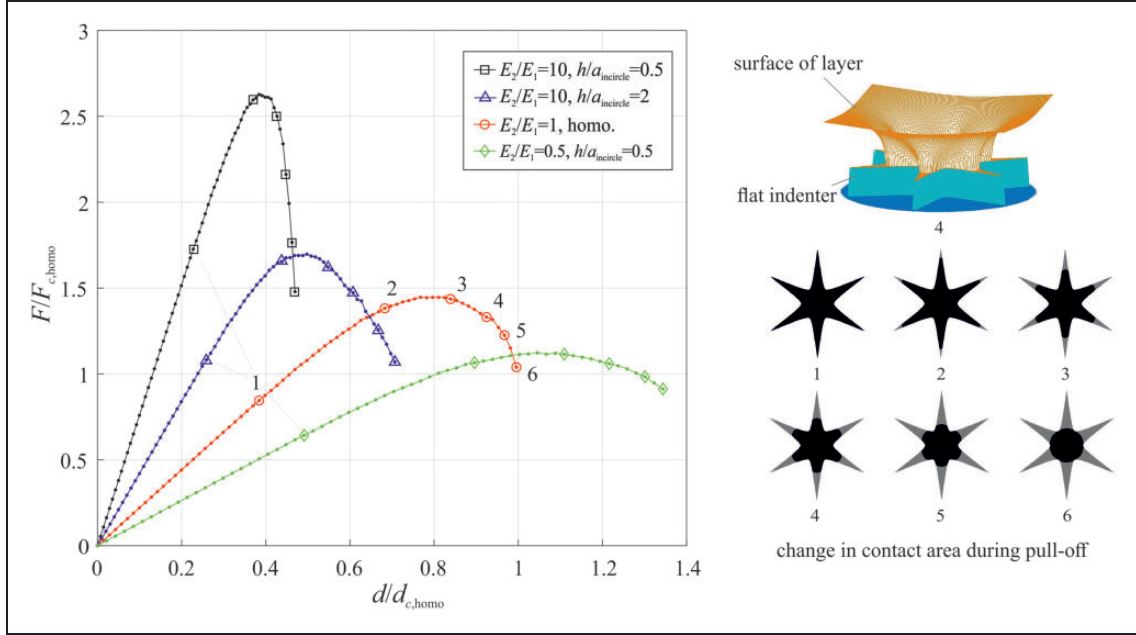


**Figure 8.** Example of adhesive detachment of a star-shaped flat indenter from a coated elastic half space. (a) Normalized tensile force vs. normalized lifting displacement. (b) Evolution of the contact zone during pull off (obtained for homogenous material).

indenters tend to detach at their outer edges first, in particular at sharp corners. It was also found that for most shapes Kendall's solution for the detachment of a cylindrical punch<sup>30</sup> applies to both force  $F_{c,homo} = \sqrt{8\pi E^* \Delta \gamma a^3}$  and displacement  $d_{c,homo} = \sqrt{2\pi \Delta \gamma a / E^*}$  at the point of final detachment. In Kendall's solution  $a$  is radius of the cylinder, while for odd shapes the incircle of the shape should be chosen. In the following, we will normalize with these two quantities and also set  $a = a_{incircle}$ .

We would like to exemplify the application of the above method by simulation of contacts of star-shaped indenters. The force–displacement relation for the homogeneous contact can be found in Figure 8. Similarly to Figures 5 and 6, the force–displacement dependencies for the star-shaped indenter were obtained by pull-off BEM simulations. For a layered system, we set  $E^* = E_1 / (1 - \nu_1^2)$ . Figure 8 shows the relations for different layer thicknesses and elastic moduli of the layers. It can be seen that both the thickness of the layer and the elastic properties have strong influence on the detachment behavior. While the dependencies of adhesive force and displacement vary significantly, the evolution of the contact area is almost universal and resembles the homogenous case: The detachment begins from points which are far from the center and at sharp corners. When the contact area shrinks to the incircle of the shape, the two surfaces separate suddenly and completely. Figure 8(b) right shows the evolution of the contact area corresponding to the six positions in all five curves.

We find that deviations from this universal evolution occur only for extreme values of the stiffness ratio. If the layer is very thin (e.g.,  $h/a_{incircle} = 0.01$ )

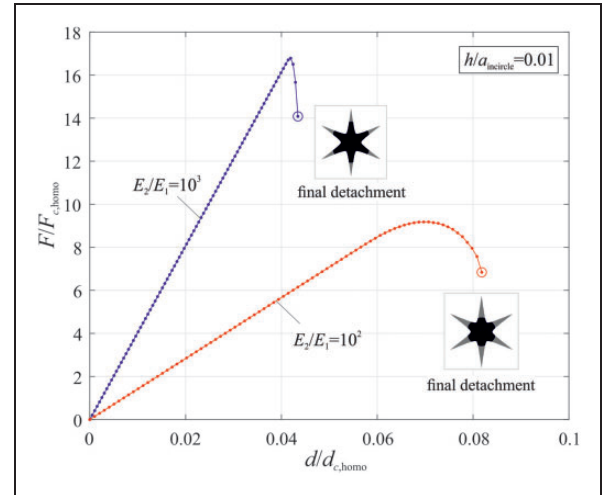


**Figure 9.** Example of adhesive detachment of a star-shaped flat indenter as in Figure 8(a) but for very thin and soft layers. Here the evolution of the contact zone deviates from the universal behavior of moderate parameters and sudden detachment occurs at larger contact area.

and soft, then we observe a different contact behavior shown in Figure 9. Here the contact area at the final detachment is significantly bigger than the incircle. The softer the layer, the larger the contact area at detachment will be.

## Conclusions

We generalized the BEM proposed in papers<sup>12,20</sup> for normal nonadhesive and adhesive contacts of an elastic half-space coated with a layer having a different elastic modulus. It is assumed that the layer is bonded

to the elastic half-space and that the contact between the layer and the indenter is frictionless. The method is based on the fundamental solution of load–displacement of the one-layer system in the Fourier domain and is valid for linear elastic contact problems. For nonadhesive contact, it is applicable for arbitrary loading. We presented the simulation procedure of the adhesive pull off. The opposite case of approaching adhesive bodies was not considered in the present paper. With the suggested BEM formulation, we carried out simulations of adhesive contacts with cylindrical flat-ended and parabolic indenters and compared the results with available asymptotic analytic solutions. We found that numerical results coincide with all available analytical results in the regions of their validity. We displayed two sample applications of non-axisymmetric contacts—the indentation of a square punch and the pull off of a star-shaped flat-ended indenter. In both cases, nontrivial behavior has been observed.

### Declaration of Conflicting Interests

The author(s) declared no potential conflicts of interest with respect to the research, authorship, and/or publication of this article.

### Funding

The author(s) disclosed receipt of the following financial support for the research, authorship, and/or publication of this article: Authors acknowledge financial support of the Deutsche Forschungsgemeinschaft (DFG PO 810-55-1) and the German ministry for research and education BMBF, grant No. 13NKE011A. This research was also partially supported by the “Toms State University competitiveness improvement program.”

### ORCID iD

Qiang Li  <https://orcid.org/0000-0001-7458-9450>

### References

1. Khadem M, Penkov OV, Yang HK, et al. Tribology of multilayer coatings for wear reduction: a review. *Friction* 2017; 5: 248–262.
2. Pogrebnyak AD, Bratushka SN, Beresnev VM, et al. Shape memory effect and superelasticity of titanium nickelide alloys implanted with high ion doses. *Russian Chem Rev* 2013; 82: 1135.
3. Bec S, Tonck A and Loubet JL. A simple guide to determine elastic properties of films on substrate from nanoindentation experiments. *Philosophic Mag* 2006; 86: 33–35. Taylor & Francis: 5347–5358.
4. Meijers P. The contact problem of a rigid cylinder on an elastic layer. *Appl Scient Res* 1968; 18: 353–383.
5. Jaffar MJ. Asymptotic behaviour of thin elastic layers bonded and unbonded to a rigid foundation. *Int J Mech Sci* 1989; 31: 229–235.
6. Constantinescu A, Korsunsky AM, Pison O, et al. Symbolic and numerical solution of the axisymmetric indentation problem for a multilayered elastic coating. *Int J Solids Struct* 2013; 50: 2798–2807.
7. Gupta PK and Walowit JA. Contact stresses between an elastic cylinder and a layered elastic solid. *J Lubricat Technol* 1974; 96: 250–257.
8. Fabrikant VI. Elementary solution of contact problems for a transversely isotropic elastic layer bonded to a rigid foundation. *J Appl Math Phys* 2006; 57: 464–490.
9. Stan G and Adams GG. Adhesive contact between a rigid spherical indenter and an elastic multi-layer coated substrate. *Int J Solids Struct* 2016; 87: 1–10.
10. Papangelo A. Adhesion between a power-law indenter and a thin layer coated on a rigid substrate. *Facta Universitatis Series Mech Eng* 2018; 16: 19–28.
11. Persson BNJ. Contact mechanics for layered materials with randomly rough surfaces. *J Phys Condens Matter* 2012; 24: 095008.
12. Pohrt R and Li Q. Complete boundary element formulation for normal and tangential contact problems. *Phys Mesomech* 2014; 17: 334–340.
13. Pohrt R and Popov VL. Adhesive contact simulation of elastic solids using local mesh-dependent detachment criterion in boundary elements method. *Facta Universitatis Series Mech Eng* 2015; 13: 3–10.
14. Argatov I, Li Q, Pohrt R, et al. Johnson-Kendall-Roberts adhesive contact for a toroidal indenter. *Proc R Soc Lond A Math Phys Eng Sci* 2016; 472(2191). DOI: 10.1098/rspa.2016.0218.
15. Li Q and Argatov I. Onset of detachment in adhesive contact of an elastic half-space and flat-ended punches with non-circular shape : analytic estimates and comparison with numeric analysis. *J Phys D Appl Phys* 2018; 145601. DOI: 10.1088/1361-6463/aab28b.
16. Popov VL, Pohrt R and Li Q. Strength of adhesive contacts: influence of contact geometry and material gradients. *Friction* 2017; 5: 308–325.
17. Li Q and Popov VL. Boundary element method for normal non-adhesive and adhesive contacts of power-law graded elastic materials. *Computat Mech* 2017; 61: 319–329.
18. Sneddon IN. Fourier-transform solution of a Boussinesq problem for a hexagonally anisotropic elastic half-space. *J Mech Appl Math* 1992; 45: 607–616.
19. Landau LD and Lifshitz EM. *Theory of elasticity. Course of theoretical physics*. 2nd ed. New York: Pergamon Press, 1970.
20. Vollebregt EAH. A new solver for the elastic normal contact problem using conjugate gradients, deflation, and an FFT-based preconditioner. *J Computat Phys* 2014; 257: 333–351.
21. Griffith AA. VI. The phenomena of rupture and flow in solids. *Philosophic Trans R Soc Lond A Math Phys Eng Sci* 1921; 221: 163–198.
22. Popov VL. Solution of adhesive contact problem on the basis of the known solution for non-adhesive one. *Facta Universitatis Series Mech Eng* 2018; 16: 93–98.
23. Ciavarella M. An approximate JKR solution for a general contact, including rough contacts. *J Mech Phys Solids* 2018; 114: 209–218.
24. Yang F. Asymptotic solution to axisymmetric indentation of a compressible elastic thin film. *Thin Solid Films* 2006; 515: 2274–2283.
25. Li Q and Popov VL. Adhesive contact between a rigid body of arbitrary shape and a thin elastic coating. *Acta Mechanica* 2019. Epub ahead of print 25 March 2019. DOI: 10.1007/s00707-019-02403-0.

26. Argatov II, Borodich FM and Popov VL. JKR adhesive contact for a transversely isotropic layer of finite thickness. *J Phys D Appl Phys* 2015; 49: 45307.
27. Shield TW and Bogy DB. Multiple region contact solutions for a flat indenter on a layered elastic half space: plane-strain case. *J Appl Mech* 1989; 56: 251–262.
28. Urquhart EE and Pindera MJ. Incipient separation between a frictionless flat punch and an anisotropic multilayered half plane. *Int J Solids Struct* 1994; 31: 2445–2461.
29. Chen LF, Urquhart EE and Pindera MJ. Microstructural effects in multilayers with large moduli contrast loaded by flat punch. *AIAA J* 2005; 43: 962–973.
30. Kendall K. The adhesion and surface energy of elastic solids. *J Phys D Appl Phys* 1971; 4: 1186.